Fast detection of the early decay in oranges using visible-LED structured-illumination imaging combined with spiral phase transform and feature-based classification model

Zhonglei Cai[1], Chanjun Sun[2], Yizhi Zhang[3,4], Ruiyao Shi[3], Junyi Zhang[1,3], Hailiang Zhang[4], Jiangbo Li[3,5*]

(1. *College of Mechanical and Electrical Engineering, Shihezi University, Shihezi 832003, Xinjiang, China*;
2. *Jiangsu Province and Education Ministry Co-sponsored Synergistic Innovation Center of Modern Agricultural Equipment, Jiangsu University, Zhenjiang 212013, Jiangsu, China*;
3. *Intelligent Equipment Research Center, Beijing Academy of Agriculture and Forestry Sciences, Beijing, 100097, China*;
4. *College of Electrical and Automation Engineering, East China Jiaotong University, Nanchang 330013, China*;
5. *National Engineering Research Center for Information Technology in Agriculture, Beijing 100089, China*)

Abstract: The early decay of citrus can cause economic and serious food safety issues. The early decayed area has no obvious visual characteristics, making effective detection of this damage very difficult for the citrus industry. This study constructed a new detection system based on visible-light emitting diode (LED) structured-illumination imaging and proposed an effective methodology combined with a spiral phase transform (SPT) algorithm for the early detection of decayed oranges. Each sample obtained three phase-shifting pattern images with phase shifts of $-2\pi/3$, 0, and $2\pi/3$ at a spatial frequency of 0.25 cycles/mm. Three strategies (i.e., the conventional three-phase-shifting method, 2-phase SPT, and 1-phase SPT) were used to demodulate the original patterned images to recover the direct component (DC) and amplitude component (AC) images. The partial least squares discriminant analysis (PLS-DA) and least squares support vector machine (LS-SVM) classification models were established based on the texture features of DC, AC, and RT (i.e. the ratio of AC to DC) images. Then, the random frog (RF) algorithm was used to simplify the optimal full-featured model. Finally, the LS-SVM model constructed using 7 texture features from the RT image obtained an average classification accuracy of 95.1% for all tested samples. This study indicates that the proposed structured-illumination imaging technique combined with 2-phase SPT and feature-based classification model can achieve the fast identification of early decayed oranges.

Keywords: oranges, early decay detection, structured-illumination imaging, spiral phase transform, classification model
DOI: 10.25165/j.ijabe.20241703.8614

Citation: Cai Z L, Sun C J, Zhang Y Z, Shi R Y, Zhang J Y, Zhang H L, et al. Fast detection of the early decay in oranges using visible-LED structured-illumination imaging combined with spiral phase transform and feature-based classification model. Int J Agric & Biol Eng, 2024; 17(3): 185–192.

1 Introduction

Citrus is rich in nutrients and has high economic value. Citrus production and trade play an important role in the global fruit industry[1]. Citrus defects have different economic importance. Some damages, such as mechanical bruises, wind erosion, and hail damage, only lead to appearance-related problems and will not evolve, but some will, especially those related to fungal or bacterial infection[2]. Early decay is the most serious postharvest disease of citrus[3,4]. Fungal spores from decayed citrus can quickly spread and infect the sound fruit in the process of storage[5]. Therefore, it is extremely important to identify these infected fruit at the early stage. However, it is a challenging task because the early infected areas can only show very slight symptoms, which makes it difficult for human eyes and traditional visual technologies (e.g., color imaging) to identify them[6,7]. Therefore, it is urgent and necessary to develop a non-destructive and fast technology for accurate detection of the early decayed citrus[8].

Many technologies, including near-infrared spectroscopy, color imaging, ultraviolet-induced fluorescence imaging, laser-light backscattering imaging, and hyperspectral imaging, have been used to identify the early decayed citrus[9]. Lorente et al.[10] proved that near-infrared spectroscopy can effectively differentiate between healthy and decayed tissues of citrus. However, this technology cannot detect the whole surface information of fruit. Therefore, the imaging technology should be more suitable for decay detection. Color imaging is a commonly used technology in citrus quality detection. However, the detection rate of this technology for early decay is low, because the external features of early decayed areas are similar to those of healthy tissues. Kurita et al.[11] used ultraviolet-induced fluorescence imaging to detect the decayed citrus. Due to

Received date: 2023-10-31 **Accepted date:** 2024-03-21
Biographies: Zhonglei Cai, PhD candidate, research interest: optical methods in rapid and non-destructive detection of quality and safety in agricultural products, Email: 3083377438@qq.com; **Chanjun Sun**, PhD, Professor, reserch interest: optical properties and spectral detection of agricultural products, Email: chanjun.sun@ujs.edu.cn; **Yizhi Zhang**, MS, reserch interest: control theory and control engineering, Emai: 929324633@qq.com; **Ruiyao Shi**, MS, research interest: computer vision technology, Email: shiry@nercita.org.cn; **Junyi Zhang**, MS, research interest: non-destructive testing of quality of agricultural products using optical sensing technology, Email: 18999112144@163.com; **Hailiang Zhang**, PhD, Professor, research interest: image detection and spectral detection, Email: zhanghailiang@zju.edu.cn.
***Corresponding author: Jiangbo Li**, PhD, Researcher, research interest: non-destructive detection of quality of agricultural products. 11 Shuguang Huayuan Middle Road, Haidian District, Beijing, China. Tel: +86-13683557791, Email: lijb@nercita.org.cn.

the different decay degrees, the fluorescence of the measured area excited by ultraviolet light has different intensities. In addition, defects such as skin scratches and freezing damage[12,13], can also confuse decay detection with similar fluorescence phenomenon. Lorente et al.[6] successfully detected early decayed citrus using laser backscattering imaging. However, this technology has some limitations as the decayed area needs to be aligned with the laser. Luo et al.[14] used a hyperspectral imaging technique to detect the decayed oranges. Although the identification rate is high, this technology still needs to solve the problems of long image acquisition and processing time in order to achieve rapid detection[15].

A new Structured-illumination Reflectance Imaging (SIRI) technique has been used for defect detection in fruit[16]. Direct Component (DC) and Alternating Component (AC) images can be obtained by demodulating phase-shift images[17]. AC image encodes information of specific depth with strong resolution and contrast. This technology has been proven to detect early decay of peaches[18] and fresh bruises of pickled cucumbers[19]. Li et al.[20] and Cai et al.[8] have successfully detected the early decayed oranges using the SIRI technique combined with the traditional three-phase shift demodulation method. Although this demodulation method can effectively retrieve DC and AC images, it requires at least three images with accurate phase shift offset, which needs a long image acquisition time, so it is difficult for real-time implementation in practice.

As analyzed above, many techniques have been applied to detect decayed citrus fruit. With these techniques, SIRI provides a new detection mode. To overcome the shortcomings of the traditional three-phase-shifting method in detection speed, the spiral phase transform (SPT) was used in this study to demodulate the pattern image based on 1-2 phase-shift images. SPT demodulation requires fewer patterned images and does not require accurate phase shifts. It reduces image acquisition time and provides a foundation for the demodulation of online devices.

The objectives of this study were to 1) demodulate the raw images obtained in the visible-LED SIRI system; 2) establish classification models (PLS-DA and LS-SVM) based on demodulated images; 3) evaluate the feasibility of classification models for detecting decayed oranges. This study was performed with the following steps: 1) the structured-illumination reflectance images of oranges were acquired using a visible-LED SIRI system under the sinusoidal modulation illumination at the spatial frequency of 0.25 cycles/mm; 2) three demodulation methods (i.e., three-phase-shifting, 2-phase SPT and 1-phase SPT) were used to recover DC and AC images from the original pattern images; 3) extract and optimize texture features of DC, AC, and RT images; 4) the classification models were developed for distinguishing decayed ones from healthy oranges; 5) evaluate the performance of classification models.

2 Materials and methods

2.1 Orange samples

Oranges (Newhall Navel Orange) were used as experimental samples considering their important economic value in the citrus industry. 290 healthy samples were purchased from a local supermarket in Beijing in December 2021. In these samples, 160 samples were made as decayed samples. The main steps of decayed sample preparation are shown in Figure 1. Firstly, orange naturally infected by fungi *Penicillium digitatum* was collected as shown in Figure 1a. Secondly, fungal spores were dissolved in water to form a spore solution as shown in Figure 1b. Thirdly, as shown in Figure 1c, artificial vaccination of healthy samples. Finally, the inoculated samples were stored in a storage cabinet (HSP-250BEII, Kuntian Laboratory Instrument Co., Ltd., Shanghai, China) with a temperature of 25°C and a relative humidity of 99% for a period of 3 days, as shown in Figure 1d. A typical sample with early decay symptoms is shown in Figure 1e. As can be observed, the decaying area has similar color characteristics to the surrounding healthy tissue. However, in terms of texture, the decayed area is usually softer than sound skin[21,22]. For all samples, the Kennard Stone (KS) algorithm[23] was used to divide the samples, 100 healthy and 100 infected samples were selected as the training set to develop the classification algorithms, while the remaining 90 samples (30 healthy and 60 infected samples) were used as the test set to evaluate the algorithms.

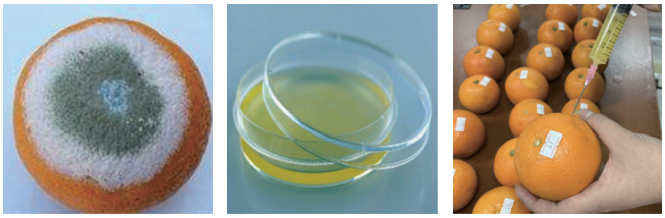

a. Infected fruit b. Fungal solution c. Fungus injection

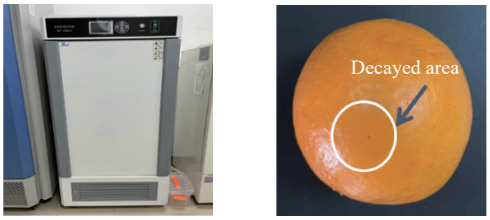

d. Constant temperature humidity chamber e. Decayed area

Figure 1 Preparation of orange samples infected by *Penicillium digitatum*

2.2 SIRI system and image acquisition

A visible-LED SIRI system, as shown in Figure 2, was developed to obtain original stripe images. This system mainly includes a digital light projector (DLP4500, Texas Instruments, USA), a monochrome camera (MV-CS050-10GM, Hikrobot Intelligent Technology Co., Ltd., Hangzhou, China) with a focusing lens (MVL-MF1628M-8MP, Hikrobot Intelligent Technology Co., Ltd., Hangzhou, China), a set of polarizers (PL-D50, RAYAN Technology Co., Ltd., China), a long wave pass filter (GCC-300701, Daheng New Epoch Technology Inc., Beijing, China) and a computer that controls the SIRI system. The projector was located at the bottom left of the camera, with a tilt angle of 15°. A set of linear polarizers was used to suppress specular reflection. A bandpass filter was installed in front of the lens, with a central wavelength of 680 nm[3]. The projector and the camera were controlled by the computer. The whole system except the computer was placed inside the black box to avoid the interference of ambient light.

Image demodulation typically requires three images with different phase-shift modes[24]. In this study, three phase-shifted sinusoidal patterns with phase offsets of $-2\pi/3$, 0, and $2\pi/3$ at the spatial frequency 0.25 cycle/mm, which were generated in the MATLAB (The Mathworks, Inc., Natick, MA, USA), were used. The spatial frequency was decided based on an earlier study[8]. During Structured-illumination (SI) image acquisition, each orange

was placed on the sample stage. The camera synchronously captures images when the projector projects sinusoidal patterns onto the sample. In this way, 3 SI images were acquired for each sample. Hence, a total of 870 SI images for 290 samples were collected in this study.

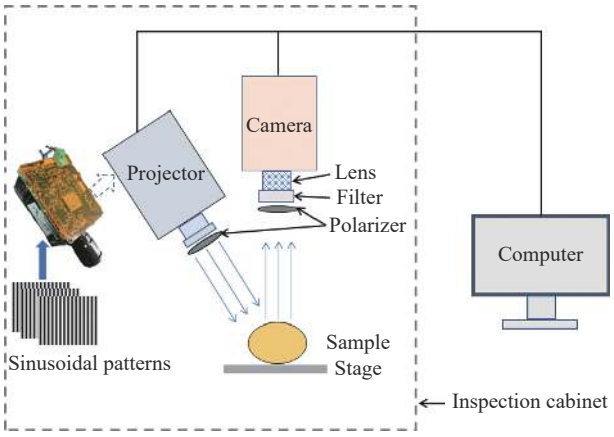

Figure 2 Schematic diagram of the developed visible-LED structured-illumination reflectance imaging system

2.3 Demodulation of pattern images

The acquired original phase-shifting images need to be demodulated to obtain DC and AC images without fringes. DC image is equivalent to an image obtained under conventional uniform illumination with zero space frequency[25]. AC image provides a measure of light attenuation within tissues due to optical properties (i.e., absorption and scattering) and encodes depth information. In the following study, three methods were studied, including the classical three-phase-shifting approach, 2-phase SPT, and 1-phase SPT.

2.3.1 Three-phase-shifting demodulation

The three-phase-shifting method is used to demodulate fringe patterns due to its high accuracy and simplicity. This method requires at least 3 pattern images with accurate phase offsets. Its definition is as follows:

$$I_k = I_{DC}(x,y) + I_{AC}(x,y)\cos[\varphi(x,y)+\theta_k],\ \ k=1,2,3 \tag{1}$$

where, $I_{DC}(x, y)$, $I_{AC}(x, y)$, and $\varphi(x, y)$ correspond to DC, AC, and phase images, respectively; θ_k is the phase offset, which can be set to $-2\pi/3$, 0, and $2\pi/3$ for k=1, 2, and 3, respectively. The demodulation equations for AC, DC, and RT images are as follows:

$$\mathrm{AC} = \frac{\sqrt{2}}{3}\left[(I_1-I_2)^2+(I_2-I_3)^2+(I_3-I_1)^2\right]^{\frac{1}{2}} \tag{2}$$

$$\mathrm{DC} = \frac{1}{3}(I_1+I_2+I_3) \tag{3}$$

$$\mathrm{RT} = \frac{\mathrm{AC}}{\mathrm{DC}} \tag{4}$$

where, I_1, I_2, and I_3 represent images with different phase offsets, respectively. Although this method only requires simple algebraic operations, it requires three patterned images with accurate phase offset. Long-time image acquisition cannot meet the requirements of online detection, and accurate phase offset is also difficult to achieve in practice.

2.3.2 Spiral Phase Transform

Spiral phase transform (SPT) is a two-dimensional extension of the traditional one-dimensional Hilbert transform (HT)[26]. HT is an important tool for constructing analytical signals in signal processing[22]. When processing two-dimensional fringe patterns, HT is implemented line by line and column by column, while SPT can be used to process fringe patterns in any direction. The two-dimensional signum function, denoted by Sgn(u, v), also known as spiral phase function (SPF), is used in SPT for the two-dimensional Hilbert transform, which is defined as follows:

$$\mathrm{Sgn}(u,v) = (u+iv)(u^2+v^2)^{-\frac{1}{2}} \tag{5}$$

where, u and v represent frequency coordinates in the Fourier space, and i is the imaginary unit. SPT includes three steps: two-dimensional Fourier transform, spiral phasor multiplication in Fourier space, and two-dimensional inverse Fourier transform, which is defined as follows:

$$\$\{[]\} = \mathrm{IFT}\{\mathrm{Sgn}(u,v)\mathrm{FT}\{[]\}\} \tag{6}$$

where, FT and IFT represent the two-dimensional Fourier transform and two-dimensional inverse Fourier transform, respectively, and the operator×represents the multiplicative sign. The $ represents the SPT. The precondition for SPT demodulation of the sinusoidal pattern is to eliminate its DC term, which can be obtained by subtracting the two-phase shifted sinusoidal patterns. For simplicity, assume two phase-shifted images I_1 and I_2 as follows:

$$I_1 = I_{DC} + I_{AC}\cos(2\pi f_x + \varphi_1) \tag{7}$$

$$I_2 = I_{DC} + I_{AC}\cos(2\pi f_x + \varphi_2) \tag{8}$$

where, φ_1 and φ_2 represent different phase angles, respectively, and f_x represents the spatial frequency along the x-axis. The following method is used for demodulation, which is called 2-phase SPT. The DC, AC, and RT images can also be recovered from two phase-shifted patterns by SPF and SPT, respectively.

$$\mathrm{AC} \cong \left[2\sin\left(\frac{\varphi_2-\varphi_1}{2}\right)\right]^{-1}\sqrt{(I_1-I_2)^2+|\$(I_1-I_2)|^2} \tag{9}$$

$$\mathrm{DC} = \frac{1}{2}\mathrm{IFT}\left[\mathrm{FT}(I_1+I_2) - \mathrm{icot}\left(\frac{\varphi_2-\varphi_1}{2}\right)\mathrm{Sgn}(u,v)\mathrm{FT}(I_1-I_2)\right] \tag{10}$$

$$\mathrm{RT} = \frac{\mathrm{AC}}{\mathrm{DC}} \tag{11}$$

For 1-phase SPT demodulation, DC removal can be completed by applying a high pass filter. The pattern image without DC can be expressed as follows:

$$I_3 = I_{AC}\cos(2\pi f_x + \varphi) \tag{12}$$

where, f_x denotes the spatial frequency along the x-axis, and φ is the phase offset. The amplitude AC can be obtained from the following equation:

$$\mathrm{AC} \cong \sqrt{I_3^2+|\$(I_3)|^2} \tag{13}$$

More details about SPT demodulation can be found in the research from Lu et al.[27].

2.4 Feature extraction and optimization

Gray-level co-occurrence matrices (GLCM) and histogram statistics (HS) methods were used to extract texture features from DC, AC, and RT images. More specifically, 14 texture statistical features were extracted from each image in each of the four directions based on GLCM proposed by Haralick et al.[28] These parameters mainly involved angular second moment, contrast, correlation, sum of squares: variance, inverse difference moment, sum average, sum variance, sum entropy, entropy, difference variance, difference entropy, information measures of correlation as

well as maximal correlation coefficient. HS was an effective method commonly used in texture analysis[29]. 8 features based on HS were extracted, including mean value, standard deviation, histogram mode, histogram entropy, upper bound, lower bound, histogram kurtosis, and histogram skewness. Thus, 64 features were extracted from each image.

Because not all features have a positive effect on identifying the infected oranges, the random frog (RF)[30] algorithm was employed to determine the informative feature features in this study. It computes a selection probability of each variable. After N iterations, a total of N variable subsets can be obtained. The frequency for the jth variable, j=1, 2, …, p, to be selected in these N variable subsets was denoted by N_j. The equation for the selection probability of each variable is as follows:

$$\text{Prob}_j = \frac{N_j}{N}, \quad j = 1, 2, ..., p \tag{14}$$

In this work, the numerical value of N was set to 10 000.

2.5 Classification models

In this study, PLS-DA and LS-SVM models were established to determine an appropriate classifier. Using the principle of partial least squares regression, a regression model between features and response values can be established. A discrimination threshold was set in the PLS-DA model. When the predicted value of PLS-DA model is greater than this threshold, it belongs to the healthy class, otherwise, it belongs to the decayed class[31]. Compared with SVM, LS-SVM can simplify the computational complexity and improve the computational speed[32]. The main parameters γ and σ^2 were determined by 10-fold cross-validation and grid optimization. All codes were developed using MATLAB R2020b (The MathWorks, Inc., Natick, Massachusetts, United States).

2.6 Identification of decayed oranges

The flow chart is shown in Figure 3. Firstly, based on the developed SIRI system, three phase-shifting images were collected for each sample at the spatial frequency of 0.25 cycles/mm. Then, three demodulation methods (i.e., traditional three-phase-shifting approach, 2-phase SPT, and 1-phase SPT) were used to obtain DC and AC images. Note that only AC can be obtained by 1-phase SPT demodulation. For three-phase-shifting demodulation, three patterned images with phase offsets of $-2\pi/3$, 0, and $2\pi/3$ were used. For 2-phase SPT and 1-phase SPT, the first two images and the first image were used respectively. Thus, 7 types of images can be obtained for each sample. Using DC and AC images, the ratio image (RT) was also generated. For each image (DC, AC, and RT) obtained from three demodulation methods, 64 texture features based GLCM and HS were extracted and RF algorithm was used to optimize these features. The full features and the optimized features were used as inputs to establish PLS-DA and LS-SVM classification models for comparative analysis.

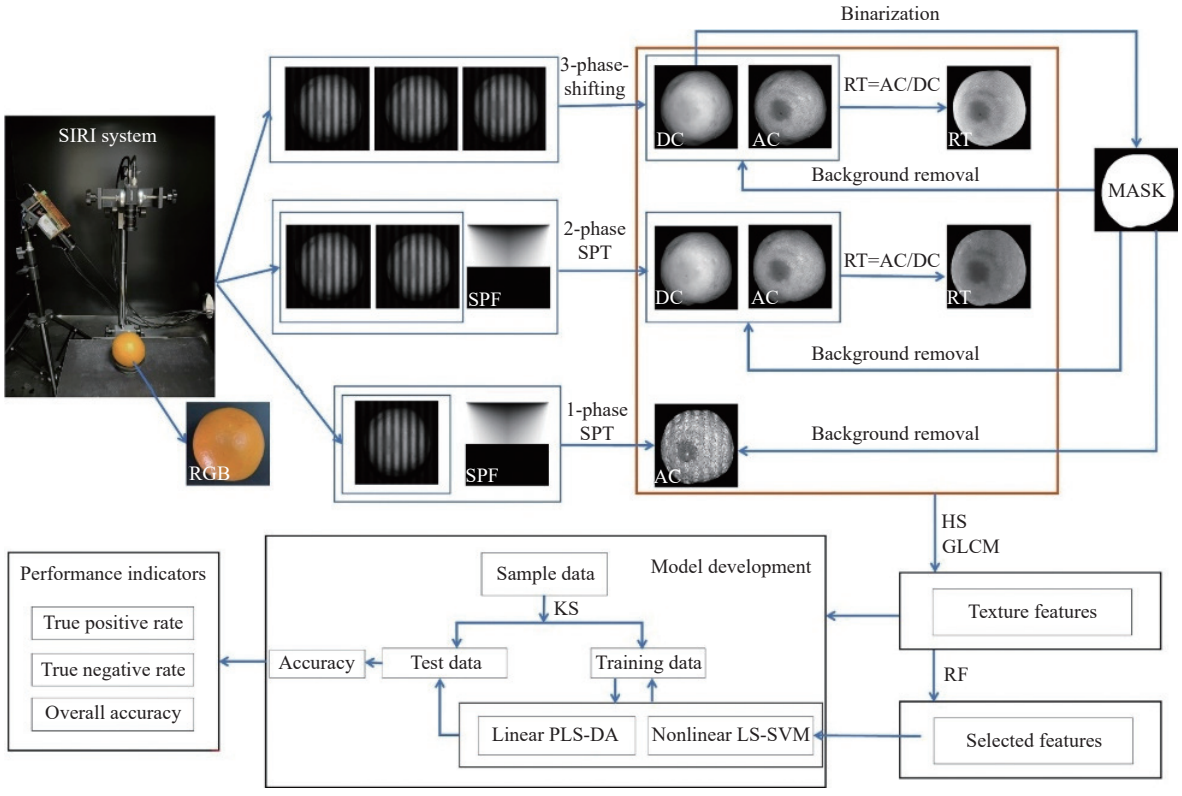

Figure 3 Detailed flow chart for detection of decayed oranges

The true positive rate (TPR), true negative rate (TNR), and overall accuracy (ACC) are evaluation indicators of model performance. The TPR and TNR correspond to the classification accuracy of decayed oranges and healthy oranges, respectively, and the ACC represents the overall classification accuracy. According to the classification results, the most appropriate input image and classifier were selected. Three indicators can be calculated as follows:

$$\text{TPR} = \frac{\text{TP}}{\text{TP} + \text{FN}} \times 100\% \tag{15}$$

$$\text{TNR} = \frac{\text{TN}}{\text{TN} + \text{FP}} \times 100\% \tag{16}$$

$$\text{ACC} = \frac{\text{TP} + \text{TN}}{\text{TP} + \text{TN} + \text{FP} + \text{FN}} \times 100\% \tag{17}$$

where, TP is the number of decayed oranges correctly classified, FN

is the number of decayed oranges incorrectly classified as healthy, TN is the number of the healthy oranges correctly classified, and FP is the number of the healthy oranges incorrectly classified as decayed.

3 Results and discussion

3.1 Analysis of demodulated images

For two typical early decayed oranges and one healthy orange, the demodulation results obtained using three-phase-shifting method, 2-phase SPT, and 1-phase SPT are shown in Figure 4. The RGB image and RT image were also shown for comparison. As can be seen, it is difficult to distinguish between decayed oranges and healthy oranges because of similar characteristics. Observing the demodulated images obtained by the three-phase-shifting method, the decayed area in the DC image, which is equivalent to the zero frequency diffuse illumination image, only shows a very slight (almost invisible) gray level change. On the contrary, the characteristics of the decayed areas in the AC image are obvious. This intensity difference is more significant in RT images, which is attributed to the more uniform light distribution on the surface of the spherical orange in the RT image. In AC and RT images, the decayed area has a lower gray value than the sound area. The demodulated image obtained from 2-phase SPT is consistent with the appeal. It showed that 2-phase SPT can be effectively used for the demodulation of pattern images and achieved good demodulation performance.

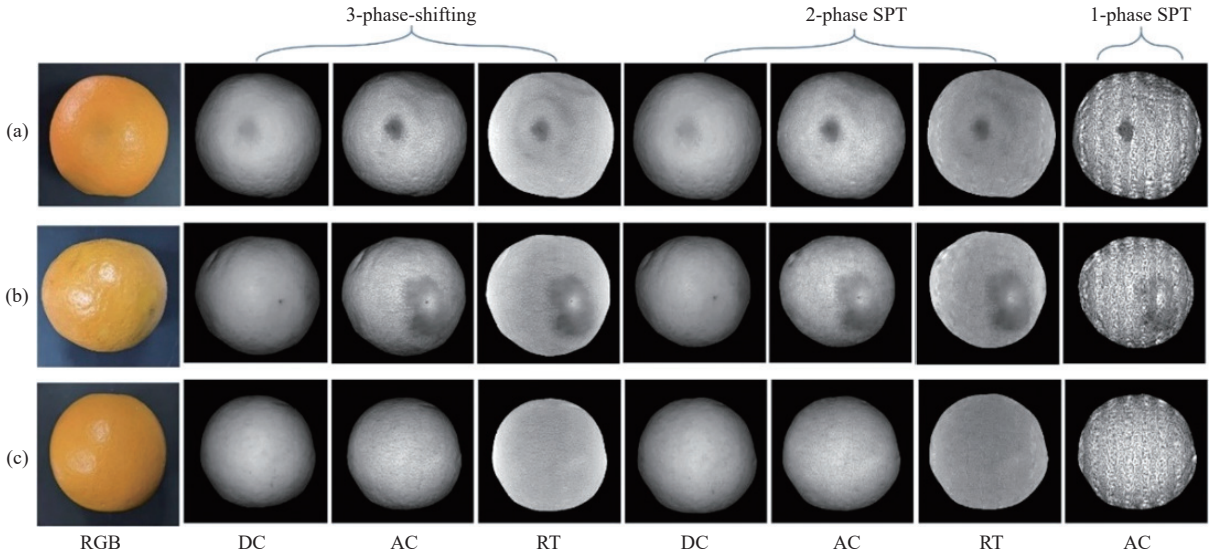

Note: (a) represents the sample with the decayed area at the center, (b) represents the sample with the decayed area at the edge, and (c) represents the healthy sample.

Figure 4 RGB images of typical samples, the corresponding direct component (DC) and alternating component (AC) images obtained by three demodulation methods, and the ratio image (RT)

In 1-phase SPT, only AC images can be obtained after demodulation, as a high-pass filter was used to remove DC. Compared with the above two methods, however, the AC image obtained by 1-phase SPT demodulation has obvious residual stripes and noises. This may be because it is difficult to choose the appropriate type and size of filter for 1-phase SPT. Traditional three-phase-shifting demodulation and 2-phase SPT methods can avoid the filter selection issue by subtracting two phase-shift images. Although the AC image demodulated by 1-phase SPT has low image quality, the decayed area has been significantly enhanced and can be clearly observed. Moreover, these residual fringes and noises can be easily reduced or eliminated by simple smooth filtering preprocessing. The most important thing is that 1-phase SPT can realize image demodulation by using only one pattern image, so it has a faster image processing speed, which is more attractive in real-time decayed orange detection. Therefore, AC image demodulated by 1-phase SPT was also used for subsequent feature extraction and modeling analysis.

In practice, the degree of decay and the position of the decayed area in the image is unpredictable, which is an unavoidable problem. In terms of the two decayed samples being exemplified, the first sample has a small decay area and is located in the middle of the orange as shown in Figure 4a. The second sample has a large decay area and is located at the edge of the orange as shown in Figure 4b. Moreover, the latter has a lighter degree of decay, which can be observed from the DC image of the two samples. By observing all AC and RT images in Figure 4, it can be found that the performance of the three demodulation methods will not be affected by the size, and location of the decay region of oranges, further demonstrating the effectiveness of the proposed SIRI technique and SPT demodulation method.

3.2 Classification results based on full features

In order to further compare the performance of demodulation methods and develop effective classification algorithms, PLS-DA and LS-SVM models were established based on texture features extracted from AC, DC, and RT images of samples. Table 1 lists the classification results of two classifiers for decayed and healthy samples.

In the three-phase-shifting method, the PLS-DA model obtained the accuracies of 83.3%, 88.9%, and 95.6% corresponding to DC, AC, and RT images, respectively, when the number of optimal LVs was 14, 15, and 20. LS-SVM model obtained the accuracies of 84.4%, 86.7%, and 97.8% corresponding to DC, AC, and RT images, respectively, when the optimal combinations of (γ/σ^2) were (485 989.7/7557.8), (90 026.6/10 393.4), and (7175.4/3896.6). In 2-phase SPT, PLS-DA model obtained the accuracies of 81.1%, 85.6%, and 93.3% corresponding to DC, AC, and RT images, respectively, when the number of optimal LVs was 20, 19, and 14. LS-SVM model obtained the accuracies of 82.2%, 86.7%, and 96.7% corresponding to DC, AC, and RT

images, respectively, when the optimal combinations of (γ/σ^2) were (968 798.8/12 182.9), (78 141.1/21 299.4) and (177 028 840.7/2 825 437.7). In 1-phase SPT, PLS-DA model obtained the accuracies of 82.2% based on AC images and when the optimal LV number of 19. LS-SVM model obtained the accuracies of 83.3% based on AC images and the optimal (γ/σ^2) combinations of (2131.9/1526.5). These results indicated that these two models can be used to classify decayed ones from healthy oranges. Furthermore, almost all LS-SVM models achieved better classification accuracy than PLS-DA models with the same inputs, which showed that the LS-SVM model was a better classifier for the detection of decayed oranges.

Table 1 Classification results of oranges based on full-feature PLS-DA and LS-SVM models with different demodulation methods and input data, and the optimal classification results with selected seven features

Methods		Input data	Models	LVs	($\gamma/\sigma2$)	Calibration set					Test set				
						Decay (100)	Healthy (100)	TPR/%	TNR/%	ACC/%	Decay (60)	Healthy (30)	TPR/%	TNR/%	ACC/%
Full features	Three-phase-shifting	DC	PLS-DA	14	/	93	97	93.0	97.0	95.0	47	28	78.3	93.3	83.3
			LSSVM	/	485 989.7/7557.8	98	99	98.0	99.0	98.5	47	29	78.3	96.7	84.4
		AC	PLS-DA	15	/	91	96	91.0	96.0	93.5	54	26	90.0	86.7	88.9
			LSSVM	/	90 026.6/10 393.4	93	100	93.0	100.0	96.5	49	29	81.7	96.7	86.7
		RT	PLS-DA	20	/	97	98	97.0	98.0	97.5	56	30	93.3	100.0	95.6
			LSSVM	/	7175.4/3896.6	98	99	98.0	99.0	98.5	58	30	96.7	100.0	97.8
	2-phase SPT	DC	PLS-DA	20	/	93	97	93.0	97.0	95.0	44	29	73.3	96.7	81.1
			LSSVM	/	968 798.8/12 182.9	96	99	96.0	99.0	97.5	45	29	75.0	96.7	82.2
		AC	PLS-DA	19	/	98	96	98.0	96.0	97.0	49	28	81.7	93.3	85.6
			LSSVM	/	78 141.1/21 299.4	97	98	97.0	98.0	97.5	49	29	81.7	96.7	86.7
		RT	PLS-DA	14	/	96	98	96.0	98.0	97.0	54	30	90.0	100.0	93.3
			LSSVM	/	177 028 840.7/2 825 437.7	98	100	98.0	100.0	99.0	57	30	95.0	100.0	96.7
	1-phase SPT	AC	PLS-DA	19	/	91	95	91.0	95.0	93.0	46	28	76.7	93.3	82.2
			LSSVM	/	2131.9/1526.5	93	95	93.0	95.0	94.0	46	29	76.7	96.7	83.3
The selected seven features	2-phase SPT	RT	LSSVM	/	693 254.6/2568.2	97	99	97.0	99.0	98.0	57	30	95.0	100.0	96.7

Note: The value in () of Test set represents the number of samples of each type.

It can be seen from Table 1 that for the three-phase-shifting and 2-phase SPT demodulation methods, no matter the LS-SVM or PLS-DA model, RT image achieved the best classification effect, followed by AC image and DC image. The low classification accuracy of DC image is due to the fact that DC image represents the image obtained under uniform field illumination, in which the decayed area is almost invisible. The AC image represents the image containing the specific depth organization information of the sample that matches the frequency of the structural light used, and thus the decayed area can be clearly seen in the image. RT image can further enhance the characteristics of the decay area. For DC, AC, and RT images, the three-phase-shifting method has the best classification effect, followed by 2-phase SPT and 1-phase SPT. This may be because the three-phase-shifting method only involves simple algebraic operations, and the finite discrete Fourier transform in 2-phase SPT has numerical errors. The reason for the worst classification effect of 1-phase SPT is that too much noise affects accurate feature extraction in the demodulated AC image.

In conclusion, the LS-SVM model combined with the RT image obtained the optimal accuracy. Based on the LS-SVM model, the TPR, TNR, and ACC of RT images demodulated by 2-phase SPT were 95.0%, 100%, and 96.7%, respectively. The TPR, TNR, and ACC of RT images obtained by three-phase-shifting demodulation were 96.7%, 100%, and 97.8% respectively. The difference in the overall classification accuracy between the two strategies was only 1.1%. However, the former only used two pattern images, which is more conducive to the implementation of rapid detection tasks. Although 1-phase SPT demodulation has the fastest execution speed, the classification accuracy (83.3%) still needs to be improved. Therefore, in view of the detection accuracy, speed, and feasibility of online implementation, the LS-SVM model based on the feature information of RT image from 2-phase SPT analysis was considered to be the optimal model for identifying decayed oranges.

3.3 Feature selection and model optimization

The RF algorithm was used to select the optimal ones from the full 64 features. For simplicity, feature selection was only applied to the optimal LS-SVM model. Because the ranking results of characteristic variables of each RF random run may be different, the most important 50 variables in 50 random runs were studied. Among the most important 50 feature variables in each random run by RF, a total of 29 variables consistently occurred in the 50 runs, as shown in Figure 5a. Figure 5b shows the corresponding selection probability of these 29 variables in 50 runs. In order to further explore the relationship between the selected features and classification accuracy, the selection probability values of 29 features were averaged and sorted. Then, the LS-SVM classification model was constructed based on different feature numbers (i.e., 1-29).

Figure 6 shows the relationship curve between feature number and overall classification accuracy. The blue bold line represents the average accuracy of 30 modeling repetitions. In general, the accuracy increases rapidly in the first seven features, reaches 95.1% in the seventh feature, and then fluctuates slightly. Among the average accuracy of all models, the accuracy of the first 27 features is the highest, reaching 95.6%. To simplify the model, the first seven features with an overall accuracy rate of 95.1% can be used as candidate subsets of features, although they may not be globally optimal. The optimal results (96.7%) of 30 modeling attempts using the first seven features are listed in Table 1. These features include contrast, entropy, and sum entropy in the direction of 0°, entropy in the direction of 45°, difference entropy in the direction of 90°, and

contrast and entropy in the direction of 135°. The 'Contrast' texture feature reflects the intensity differences between different regions of orange in RT image. In RT image, it is very obvious that there is an important intensity difference between the decaying area and the healthy area of oranges. The difference between entropy and sum entropy, which are similar to the meaning of entropy, is a measure of the amount of information in an image. It is a measure of randomness, indicating the degree of heterogeneity or complexity of the texture in the decaying and healthy oranges.

Hyperspectral imaging was commonly used in research early decay detection of citrus. Li et al.[3] used this technique to successfully identify early decayed oranges. Four important wavelength images centered at 575, 698, 810, and 969 nm were selected to develop a fast classification method and obtained a detection accuracy of 98.6 %. Li et al.[33] proposed an algorithm for the identification of decayed oranges by combining multispectral principal component images, two-dimensional empirical mode decomposition, and watershed segmentation. The identification accuracies of decayed and healthy oranges were 97.3% and 100%, respectively. Tian et al.[7] used LW-NIR hyperspectral reflectance imaging coupled with two-band ratio and improved watershed segmentation algorithm to detect early citrus decay. The image-level detection method proposed in his study obtained a total success rate of 92% for all samples. Although hyperspectral imaging has been proven to be successful in detecting decayed citrus, the expensive equipment and time-consuming data acquisition limit its practical application. Different from hyperspectral imaging, as a novel technology, Cai et al.[8] and Li et al.[20] have successfully demonstrated the feasibility of SIRI for the detection of decayed oranges by combining the three-step phase shift demodulation. The methodology introduced in this study further accelerated the practical application of this technology.

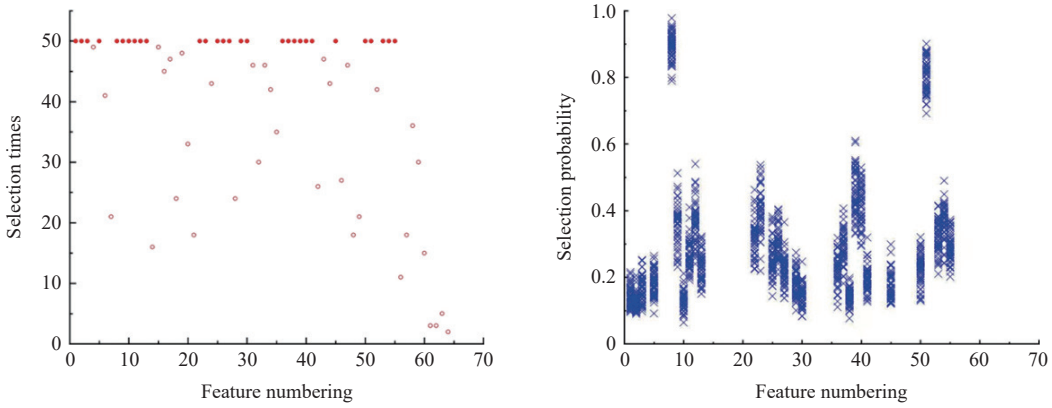

a. Selected times of each feature in 50 random runs

b. Selection probabilities of the most important 29 features in 50 random runs

Figure 5 Effective feature selection by RF algorithm

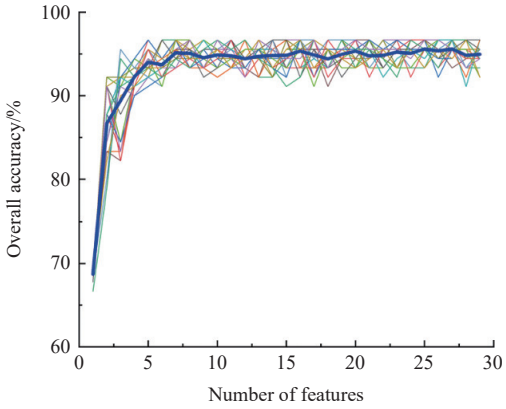

Note: In this figure, each line represents one of 30 modeling repetitions and the blue bold line represents the average accuracy of 30 modeling repetitions.

Figure 6 Relationship curve between feature number and overall classification accuracy for the selected 29 features

4 Conclusions

This study successfully demonstrated that the visible-LED SIRI technique combined with feature-based PLS-DA and LS-SVM classification models can effectively detect early decayed oranges. The proposed SPT method can be used to recover AC images using only one or two pattern images with arbitrary phase offsets. Compared with the three-phase method, 2-phase SPT method got a comparable classification performance, which makes it possible to achieve faster implementation of SIRI. Seven types of input images were obtained by three demodulation methods. 64 texture features of each type of image were extracted and 14 groups of models were constructed to classify decayed ones from healthy oranges. The classification results showed that almost all LS-SVM models were better than PLS-DA models, and RT image was the best, followed by AC and DC images. By comprehensively considering the classification accuracy and online application potential, the LS-SVM model combined with RT image obtained by 2-phase SPT demodulation achieved the highest classification accuracy of 96.7% for oranges in the test set. In addition, RF algorithm was proved to be a useful tool that can be utilized to extract the most critical features. The LS-SVM model constructed with the selected seven texture features achieved an overall classification accuracy of 95.1%. The performed work and the proposed methodology in this study can lay a solid foundation for the practical application of SIRI technology in early decayed orange classification.

Acknowledgements

This work was supported by the Outstanding Scientist Cultivation Project of Beijing Academy of Agriculture and Forestry Sciences (Grant No. JKZX202405), Jiangsu Province and Education Ministry Co-sponsored Synergistic Innovation Center of Modern Agricultural Equipment (Grant No. XTCX2001), National Natural Science Foundation of China (Grant No. 31972152; No. 32260622) and Natural Science Foundation of Jiangxi Province, China (Grant No. 20232ACB205026).

[References]

[1] Zhang H L, Chen Y, Liu X M, Huang Y F, Zhan B S, Luo W. Identification of common skin defects and classification of early decayed citrus using hyperspectral imaging technique. Food Analytical Methods, 2021; 14(6): 1176–1193.

[2] Cubero S, Lee W S, Aleixos N, Albert F, Blasco J. Automated systems based on machine vision for inspecting citrus fruits from the field to postharvest-a review. Food Bioprocess Technology, 2016; 9(10): 1623–1639.

[3] Li J B, Huang W Q, Tian X, Wang C P, Fan S X, Zhao C J. Fast detection and visualization of early decay in citrus using Vis-NIR hyperspectral imaging. Computers and Electronics in Agriculture, 2016; 127: 582–592.

[4] Golzarian M R, Ghooshkhaneh N G, Mamarabadi M. Detection and classification of citrus green mold caused by *Penicillium digitatum* using multispectral imaging. Journal of the Science of Food and Agriculture, 2018; 98(9): 3542–3550.

[5] Lorente D, Zude M, Regen C, Palou L, Gomez-Sanchis J, Blasco J. Early decay detection in citrus fruit using laser-light backscattering imaging. Postharvest Biology and Technology, 2013; 86: 424–430.

[6] Lorente D, Zude M, Idler C, Gómez-Sanchis J, Blasco J. Laser-light backscattering imaging for early decay detection in citrus fruit using both a statistical and a physical model. Journal of Food Engineering, 2015; 154: 76–85.

[7] Tian X, Fan S X, Huang W Q, Wang Z L, Li J B. Detection of early decay on citrus using hyperspectral transmittance imaging technology coupled with principal component analysis and improved watershed segmentation algorithms. Postharvest Biology and Technology, 2020; 161: 111071.

[8] Cai Z L, Huang W Q, Wang Q Y, Li J B. Detection of early decayed oranges by structured-illumination reflectance imaging coupling with texture feature classification models. Frontiers in Plant Science, 2022; 13: 952942.

[9] Mei M W, Li J B. An overview on optical non-destructive detection of bruises in fruit: technology, method, application, challenge and trend. Computers and Electronics in Agriculture, 2023; 213: 108195.

[10] Lorente D, Escandell-Montero P, Cubero S, Gómez-Sanchis J, Blasco J. Visible-NIR reflectance spectroscopy and manifold learning methods applied to the detection of fungal infections on citrus fruit. Journal of Food Engineering, 2015; 163: 17–24.

[11] Kurita M, Kondo N, Shimizu H, Ling P, Falzea P D, Shiigi T, et al. A double image acquisition system with visible and UV LEDs for citrus fruit. Journal of Robotics and Mechatronics, 2009; 21(4): 533–540

[12] Slaughter D C, Obenland D M, Thompson J F, Arpaia M L, Margosan D A. Non-destructive freeze damage detection in oranges using machine vision and ul-traviolet fluorescence. Postharvest Biology and Technology, 2008; 48: 341–346.

[13] Obenland D, Margosan D, Smilanick J L. Ultraviolet fluorescence to identify navel oranges with poor peel quality and decay. HortTechnology, 2010; 20(6): 991–995.

[14] Luo W, Fan G Z, Tian P, Dong W T, Zhang H L, Zhan B S. Spectrum classification of citrus tissues infected by fungi and multispectral image identification of early rotten oranges. Spectrochim Acta Part A: Molecular and Biomoleculr Spectroscopy, 2022; 279: 121412.

[15] Fan S X, Liang, X T, Huang W Q, Zhang V J, Pang Q, He X, et al. Real-time defects detection for apple sorting using NIR cameras with pruning-based YOLOV4 network. Computers and Electronics in Agriculture, 193: 106715.

[16] Lu Y Z, Li R, Lu R F. Structured-illumination reflectance imaging (SIRI) for enhanced detection of fresh bruises in apples. Postharvest Biology and Technology, 2016; 117: 89–93.

[17] Cai Z L, Sun C J, Zhang H L, Zhang Y Z, Li J B. Developing universal classification models for the detection of early decayed citrus by structured-illumination reflectance imaging coupling with deep learning methods. Postharvest Biology and Technology, 2024; 210: 112788.

[18] Sun Y, Lu R F, Lu Y Z, Tu K, Pan L Q. Detection of early decay in peaches by structured illumination reflectance imaging. Postharvest Biology and Technol, 2019; 151: 68–78.

[19] Lu Y Z, Lu R F, Zhang Z. Detection of subsurface bruising in fresh pickling cucumbers using structured-illumination reflectance imaging. Postharvest Biology and Technology, 2021; 180: 111624.

[20] Li J B, Lu Y Z, Lu R F. Detection of early decay in navel oranges by structured-illumination reflectance imaging combined with image enhancement and segmentation. Postharvest Biology and Technology, 2023; 196: 112162.

[21] Barmore C R, Brown G E. Polygalacturonase from citrus fruit infected with *Penicillium italicum*. Phytopathology, 1981; 71: 328–331

[22] Baranowski P, Mazurek W, Pastuszka-Wozniak J. Supervised classification of bruised apples with respect to the time after bruising on the basis of hyperspectral imaging data. Postharvest Biology and Technology, 2013; 86: 249–258.

[23] Sun Y, Yuan M, Liu X Y, Su M, Wang L L, Zeng Y Z, et al. A sample selection method specific to unknown test samples for calibration and validation sets based on spectra similarity. Spectrochim Acta A: Molecular and Biomolecular Spectroscopy, 2021; 258: 119870.

[24] Lu Y Z, Lu R F. Structured-illumination reflectance imaging for the detection of defects in fruit: Analysis of resolution, contrast and depth-resolving features. Biosystems Engineering, 2019; 180: 1–15.

[25] Li J B, Lu Y Z, Lu R F. Identification of early decayed oranges using structured-illumination reflectance imaging coupled with fast demodulation and improved image processing algorithms. Postharvest Biology and Technology, 2024; 207: 112627.

[26] Larkin K G, Bone D J, Oldfield M A. Natural demodulation of two-dimensional fringe patterns. I. General background of the spiral phase quadrature transform. Journal of the Optical Society of America A, 2001; 18(8): 1862–1870.

[27] Lu Y Z, Li R, Lu R F. Fast demodulation of pattern images by spiral phase transform in structured-illumination reflectance imaging for detection of bruises in apples. Computers and Electronics in Agriculture, 2016; 127: 652–658.

[28] Haralick R M, Shanmugam K, Dinstein I. Textural features for image classification. IEEE Transactions on Systems, Man, and Cybernetics, 1973; SMC-3(6): 610–621.

[29] Hu J, Li D L, Duan Q L, Han, Y Q, Chen G F, Si X L. Fish species classification by color, texture and multi-class support vector machine using computer vision. Computers and Electronics in Agriculture, 2012; 88: 133–140.

[30] Li H D, Xu Q S, Liang Y Z. Random frog: An efficient eversible jump Markov chain Monte Carlo-like approach for variable selection with applications to gene selection and disease classification. Analytica Chimica Acta, 2012; 740: 20–26.

[31] Wold S, Sjöström M, Eriksson L. PLS-regression: A basic tool of chemometrics. Chemometrics and Intelligent Laboratory Systems, 2001; 58(2): 109–130.

[32] Zhang Y F, Wang Z L, Tian X, Yang X H, Cai Z L, Li J B. Online analysis of watercore apples by considering different speeds and orientations based on Vis/NIR full-transmittance spectroscopy. Infrared Physics & Technology, 2022; 122: 104090.

[33] Li J B, Zhang R Y, Li J B, Wang Z L, Zhang H L, Zhan B S, et al. Detection of early decayed oranges based on multispectral principal component image combining both bi-dimensional empirical mode decomposition and watershed segmentation method. Postharvest Biology and Technology, 2019; 158: 110986.